Nanoscale

ROYAL SOCIETY OF CHEMISTRY

MINIREVIEW

View Article Online
View Journal | View Issue

Cite this: *Nanoscale*, 2020, **12**, 7500

Substrate induced strain for on-surface transformation and synthesis

Jie Su,[a,b] Xinbang Wu,[a] Shaotang Song,[a] Mykola Telychko*[a,b] and Jiong Lu *[a,b]

Received 14th February 2020,
Accepted 11th March 2020

DOI: 10.1039/d0nr01270j

rsc.li/nanoscale

Intermolecular strain has long been used to steer and promote chemical reactions towards desired products in wet chemical synthesis. However, similar protocols have not been adopted for the on-surface synthesis on solid substrates due to the complexity of reaction processes. Recent advances in the submolecular resolution with scanning probe microscopy allow us to capture on-surface reaction pathways and to gain substantial insights into the role of strain in chemical reactions. The primary focus of this review is to highlight the recent findings on strain-induced on-surface reactions. Such substrate-induced processes can be applied to alter the chemical reactivity and to drive on-surface chemical reactions in different manners, which provides a promising alternative approach for on-surface synthesis. This review aims to shed light on the utilization of substrate-induced strain for on-surface transformation and synthesis of atomically-precise novel functional nanomaterials.

Introduction

The field of on-surface synthesis of functional nanomaterials has advanced rapidly in the past few decades.[1–6] Common strategies for the on-surface synthesis often involve the rational design of a molecular precursor combined with a judicious choice of catalytic substrates with external stimuli, which can enable versatile control over reaction pathways towards the desired final products.[3,7–12] The utilization of such bottom-up synthetic approaches has allowed the fabrication of a plethora of novel molecules and functional nanostructures with different topologies, and electronic and magnetic properties under ultra-high vacuum (UHV) conditions.[1,3,13–16] It is worth mentioning that the majority of these nanostructures are unattainable *via* conventional organic synthesis, due to their poor solubility and high reactivity under ambient conditions.[17,18] In contrast to the wet chemical synthesis conducted in the solution phase, on-surface synthesis exploits similar chemical reactions on a solid substrate, such as Ullmann, Sonogashira, Glaser coupling and cyclodehydrogenation reactions *via* dehalogenation and dehydrogenation processes.[3,19] Various carbon-based nanostructures have been synthesized *via* the on-surface synthetic strategy and subsequently characterized by scanning

[a]*Department of Chemistry, National University of Singapore, 3 Science Drive 3, Singapore 117543, Singapore. E-mail: chmtm@nus.edu.sg, chmluj@nus.edu.sg*
[b]*Centre for Advanced 2D Materials (CA2DM), National University of Singapore, 6 Science Drive 2, Singapore 117546, Singapore*

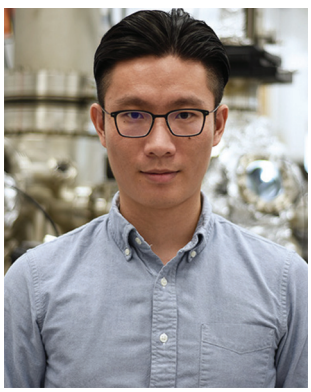

Jie Su

Dr Jie Su is a postdoctoral researcher at the Department of Chemistry, Centre for Advanced 2D Materials, National University of Singapore (NUS). He joined Assistant Professor Jiong Lu's research group in 2015 as a Ph.D. student, and received his degree in 2019. His current research topic focuses on the on-surface synthesis and characterization of graphene nanostructures using scanning tunneling microscopy and noncontact atomic force microscopy.

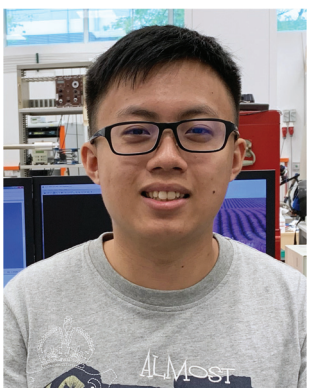

Xinbang Wu

Mr Xinbang Wu is doing his B.Sc. in materials chemistry at the Department of Chemistry, National University of Singapore. He joined Assistant Professor Jiong Lu's group in 2018. His current research interests include the synthesis and characterization of novel nanomaterials.

probe microscopy with sub-molecular resolution.[7,14,19–23] Generally, the topologies and physical properties of the final products can be tuned by the rational design of elegant molecular precursors. For instance, acene motifs are introduced in precursors for the synthesis of armchair-edged graphene nanostructures by promoting the cyclization process along the armchair direction. In contrast, methyl groups are incorporated to synthesize zigzag-edged graphene nanostructures, because additional carbon atoms are needed to close the ring along the zigzag direction.[13,23] Therefore, the precursor design constitutes the first key step for the on-surface synthesis.

Apart from the precursor design, typical on-surface synthesis also requires external stimuli *via* thermal-annealing or light irradiation to trigger intramolecular and intermolecular transformations.[1,3,13] The thermal-annealing protocol has been widely adopted to control the reaction products by varying the annealing temperature and supporting substrate (*e.g.* Au, Ag and Cu). For example, Lafferentz *et al.* reported the formation of a porphyrin-based two-dimensional (2D) framework by sequentially activating the iodine and bromine sites on the Au(111) surface. Annealing 5,15-bis(4-bromophenyl)-10,20-bis(4-iodophenyl)porphyrin (*trans*-Br_2I_2TPP) at ~400 K results in the cleavage of the iodine atoms to form a chain-like structure. The 2D framework can be subsequently formed at ~500 K by removing the bromine atoms and coupling with other chains.[24] Analogously, Cao *et al.* reported that annealing 6,11-dibromo-1,4-diphenyl-2,3-dithenoyltriphenylene (DBTP) at elevated temperatures leads to different final products, including sulfur-doped GNRs and pure-hydrocarbon GNRs.[25] Besides, light illumination can act as an alternative stimulus to induce on-surface reactions. Urgel *et al.* have demonstrated the light-induced generation of higher acene molecules on the Au(111) surface. In this case, the incident light is applied to dissociate the α-diketone moieties of precursors by exciting the n–π* transition of the molecules, resulting in the formation of unsubstituted heptacene and nonacene molecules. For the light-induced on-surface synthesis, a judicious choice of the wavelength of incident light is required to excite molecular precursors and metal substrates (to generate hot electrons by the interband transition) towards efficient transformations into the desired products.[26]

In addition to the factors aforementioned, the crystallographic symmetry and catalytic activity of the underlying substrates also play vital roles in various surface chemical reactions (Fig. 1). For example, the 10,10′-dibromo-9,9′-bianthracene (DBBA) precursor can be transformed into graphene nanoribbons (GNRs) only on certain metal substrates such as Au(111) and Cu(111).[3] In contrast, it is converted into nanographene rather than GNRs on the Cu(110) surface due to lower symmetry and higher reactivity compared to Au(111) and Cu(111). The increased reactivity of the Cu(110) surface favors the substrate–molecular interaction over the intermolecular one, which thus suppresses the Ullmann coupling pathway towards the formation of GNRs.[27] Additionally, the use of different metal substrates could also result in the formation of a covalently-bonded framework with distinct morphologies. Treier *et al.* reported that the hexaiodo-substituted CHP precursor tends to form ordered framework domains on the Ag(111) surface upon thermal annealing, while branch-like structures are preferentially formed on the Cu(111) substrate.[28] Such a difference can be attributed to the different relative energy barrier between surface diffusion and chemical reactions on these two substrates. When the diffusion prevails the reaction, the increased mobility can result in a more regular framework.

The exploration of conceptually new toolkits for steering of on-surface reactions can further accelerate the development in the field of on-surface synthesis. Mechanochemical synthesis, driven by external force/strain, is regarded as a promising alternative approach for synthesizing novel functional nanomaterials. Unfortunately, such an approach cannot be directly

Shaotang Song

Dr. Shaotang Song received his Master's degree (2014) from Beijing Institute of Technology and then obtained his PhD degree (2017) under the supervision of Professor Hiroshi Sakaguchi at Kyoto University. He joined the groups of Hiromitsu Maeda at Ritsumeikan University (2018) and Jiong Lu at National University of Singapore (2018–present) for the postdoctoral research. His current research focuses on the bottom-up on-surface synthesis and characterization of graphene nanostructures via *a combination of organic synthesis and scanning tunneling microscopy.*

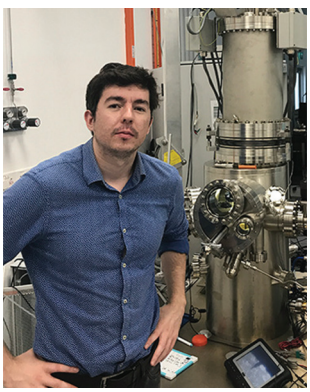

Mykola Telychko

Dr Mykola Telychko received his Master's degree (2012) at the Department of Physics of Uzhgorod, National University of Ukraine. He obtained his PhD degree (2016) under the supervision of Professor Pavel Jelínek at Institute of Physics, Academy of Science of Czech Republic. Afterwards, he joined the group of Assistant Professor Jiong Lu at the Department of Chemistry, National University of Singapore as a postdoctoral researcher (2016–present). His current research topics include studying novel 2D materials and the bottom-up synthesis of graphene-like nanostructures, by means of high-resolution scanning probe microscopy techniques.

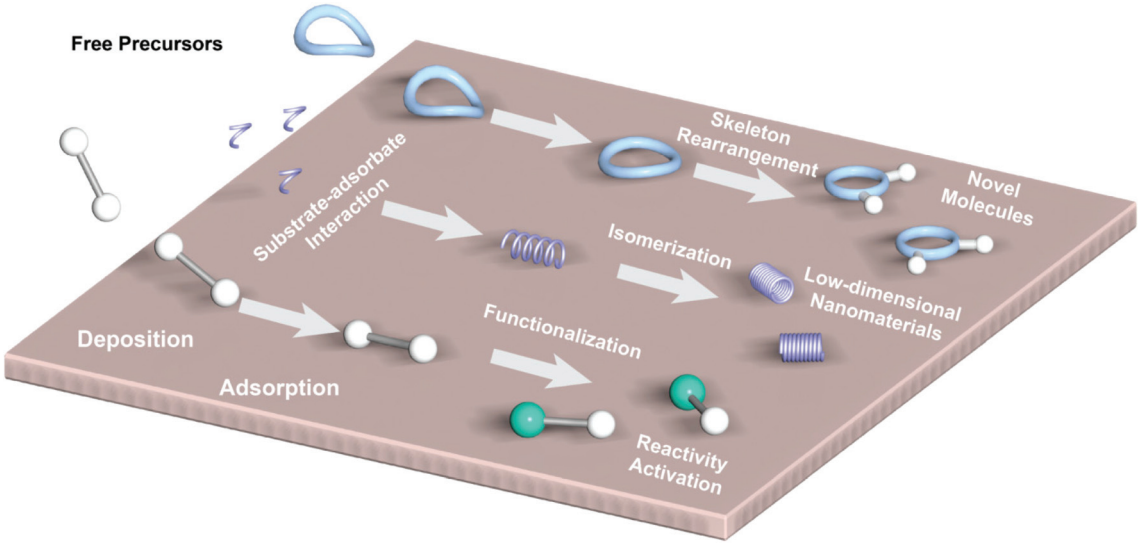

Fig. 1 On-surface synthesis of novel molecules and functional nanostructures steered by the substrate–adsorbate interaction.

applied to the on-surface synthesis because conventional methods for applying external force (*e.g.* ball milling and cavity grinding) cannot be implemented with the reactants adsorbed on a substrate. Recent progress has revealed that substrate-induced strain can be potentially exploited to drive the on-surface reaction along the desired pathway because it mimics the external mechanical stimuli used for the mechano-chemical synthesis in the solution phase.[29–33] This concept has been demonstrated in recent reports, including the strain-induced skeleton re-arrangement of different PAHs on the Cu (001) surface and strain-induced intramolecular cyclodehydrogenation of the CHP precursor towards the formation of nanographene on the Cu(111) surface.[29,34]

The complexity of molecular transformations and fine structural variations often precludes the capture of the full role of inter/intramolecular strains in reaction pathways using conventional sample-averaged characterisation techniques. In contrast, the tip-functionalised non-contact atomic force microscopy (nc-AFM) imaging technique has emerged as a powerful tool for sub-molecular resolution imaging of reaction intermediates and final products synthesized on various surfaces.[35–40] Such high-resolution imaging is achieved *via* the use of a tuning-fork-based force sensor with the tip apex decorated with a specific molecule/atom (*e.g.* carbon-monoxide (CO)). The functionalised tip oscillated with a small amplitude (<0.1 A) offers an increased sensitivity to the short-range forces in the Pauli repulsion regime. The strongest Pauli repulsion occurs over regions of high electron density (*e.g.* chemical bonds), which allows for imaging of the molecular backbone with sub-molecular resolution.[30,41–44] It is therefore accessible to trace fine conformational changes of reaction intermediates and products using this technique.[45–47]

In the following sections, we will highlight the recent progress in the strain-induced structural re-arrangement and chemical transformation on the surface. In particular, we will first discuss how intramolecular strain gives rise to the skeletal rearrangements of individual polyaromatic hydrocarbon molecules.[34] Following this, we will then describe our recent report on the strain-induced intermolecular rearrangements in extended metal–organic structures.[48] In the final part we will discuss how the crystallographic symmetry and catalytic activity of the metal substrate could alter the properties of chemically identical amine groups.[49] Appropriate utilization of substrate-induced strain could potentially enrich the existing toolbox of on-surface chemistry (Fig. 1).

Jiong Lu

Dr Jiong Lu is currently an Assistant Professor at the Department of Chemistry, Centre for Advanced 2D Materials, National University of Singapore (NUS). He received his Bachelor's degree from Fudan University (China) in 2007 and PhD degree from NUS in 2011. After that, he worked as a postdoc fellow in the Graphene Research Centre, NUS, and then joined Mike Crommie's group at the Department of Physics, UC, Berkeley, for his postdoctoral research. His current research interests include atomic-scale imaging and characterization of 2D materials and their gate-tunable devices, and single-atom catalysis for energy related applications.

Strain-induced skeletal rearrangement at the single-molecule level

Iwata and co-workers reported a strain-induced intramolecular skeletal rearrangement of polyaromatic hydrocarbons (PAHs)

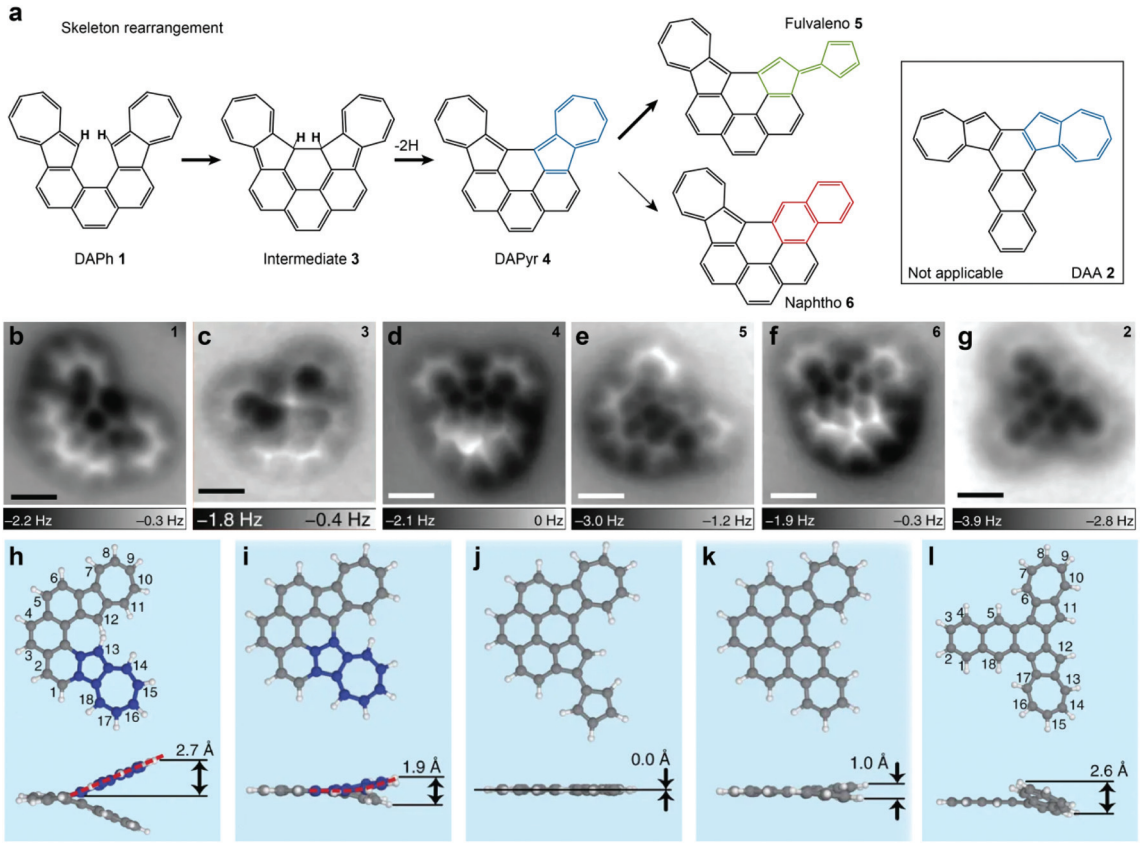

Fig. 2 (a) Reaction of DAPh **1** on Cu(001) to yield a fulvaleno-rearranged product **5** and a naphtho-rearranged product **6** *via* intermediates **3** and **4**. The DAA **2** (framed at right) is not applicable for skeletal rearrangement. (b–f) nc-AFM images of precursor DAPh **1**, intermediate **3**, cyclized DAPyr **4**, and the final products fulvaleno **5**/naphtho **6**. (g) nc-AFM image of molecule DAA **2**. Scale bar: 5 Å. (h–l) The corresponding molecular models for the top view and side view of freestanding molecules DAPh **1**, DAPyr **4**, fulvaleno **5**, naphtho **6** and DAA **2**. (Reproduced from ref. 34, Copyright 2017, with permission of Springer Nature.)

on the Cu(100) surface.[34] Two molecular precursors, diazuleno [1,2-c:2′,1′-g]phenanthrene (DAPh) **1** and diazuleno[1,2-*a*:2′,1′-*c*] anthracene (DAA) **2** (Fig. 2a), were synthesized for this study. The gas-phase DAPh monomer is highly twisted due to the steric repulsion between the two H atoms, bonded to 12- and 13-positioned C atoms respectively (Fig. 2h), while the gas-phase DAA monomer adopts a bent geometry, attributed to the steric repulsion of H atoms between 5- and 6-positions and between 17- and 18-positions (Fig. 2l). However, constant-height nc-AFM imaging (Fig. 2b and g) reveals that both of them attain a relatively flat adsorption geometry upon adsorption on the Cu(001) surface, corroborated by density functional theory (DFT) calculations. Such a surface planarization of non-flat molecular precursors may result in the accumulation of internal strain, which is expected to promote diverse skeletal rearrangements of molecules upon thermal annealing.

Several distinct products are formed upon annealing a DAPh-decorated Cu(001) substrate at different temperatures. According to the experimental observations, a reaction pathway of **1–3–4–5/6** is assumed, as illustrated in Fig. 2a. Product **3** shows a bright protrusion at the centre as elucidated by nc-AFM imaging (Fig. 2c), suggesting a non-planar adsorption geometry. The backbone of products **4** to **6**, with a flattened adsorption geometry on Cu(001), can be better visualized in the nc-AFM image (Fig. 2f). Both nc-AFM imaging and theoretical calculations indicate that products **5** and **6** are obtained through the skeletal rearrangement of one azuleno moiety in product **4** into a fulvaleno or naphtho moiety. In contrast, it is observed that the DAA **2** cannot be cyclodehydrogenated, nor be rearranged in multi-annealing processes.

DAPh **1** undergoes two types of competing rearrangements at elevated temperatures: (i) cyclodehydrogenation at ~400 K and (ii) skeletal rearrangement above 473 K. Compared to DAPh **1**, the azuleno parts of the product DAPyr **4** are distorted in free space due to the steric hindrance between the azuleno groups and the rigidity of the pyrene part (red dashed line in Fig. 2i). In addition, DFT calculations show that the newly formed six-membered carbon ring in DAPyr **4** does not have aromatic features, which suggests that the cyclodehydrogenation process is not driven by extension of the aromaticity. Moreover, the calculated flattening energy of DAPyr **4** (~0.1 to 0.17 eV) is much larger than that of DAPh **1** (~15 to 60 meV) on the Cu(001) surface, indicating that the flattened configuration of DAPyr **4** could induce a more substantial strain com-

pared to molecule **1** on the Cu(001) surface. All these observations suggest that intramolecular strain provides a driving force to promote the skeletal rearrangement of DAPyr **4** molecules.

Product **5** appears to be the most abundant species after annealing at ~520 K, which implies that the majority of azuleno moieties are converted into fulvaleno moieties rather than naphtho ones. It is noted that DFT calculations predict that the product **5** is planar in free space, indicating that the reactions **4**–**5** eliminate the strain instability in the molecule DAPyr **4** on the Cu(001) surface. In contrast, the formation of product **6** is energetically unfavourable because the flattening energy of **6** is higher (110 meV) than that of **5**. Therefore, product **6** may be rearranged into **5** in a planar manner due to the relief of intramolecular strain. The combination of nc-AFM imaging and DFT calculation allows us to reveal the roles of intramolecular strain during the on-surface process. Such strain-induced on-surface transformation provides a promising route to synthesize novel functional molecules.

Strain-induced isomerization of 1D organometallic nanostructures at room temperature

We recently reported an internal strain-induced isomerization reaction of one dimensional (1D) metal–organic chains (MOCs) on the Cu(111) surface.[48] In our study, the 1,5-dibromo-2,6-dimethylnaphthalene (DBDMN) molecule is chosen as the precursor to synthesize 1D MOCs on the Cu(111) substrate. Upon deposition on the substrate, DBDMN molecules are expected to undergo the cleavage of C–Br bonds at room temperature. As a result, σ-radicals are formed by removal of Br atoms, coordinating with the Cu adatoms on the surface to form 1D MOCs with homochiral and heterochiral configurations. However, the MOCs evolve into different configurations after annealing at room temperature for ~12 hours. These configurations are presented by newly formed dumbbell-shaped 1D MOCs, indicating that the original MOCs underwent structural rearrangement (Fig. 3a). The MOC isomers before and after room-temperature annealing are referred to as strained and relaxed ones, respectively.

nc-AFM imaging with a CO-decorated tip was performed to unveil structural transitions from the strained to the relaxed MOC. However, it is challenging to resolve the chemical backbone of the strained MOCs because the most substantial Pauli repulsion occurs over protruding methyl groups located at the 2- and 6-positions of DBDMN monomers. To overcome such a challenge, a controllable tip-induced dehydrogenation was performed, *via* STM scanning at an elevated bias voltage of V_s > 1.6 V. This process allows for the removal of the protruding hydrogen atoms of methyl groups without inducing any intramolecular rearrangements or alternations of the C–Cu–C bonding motif. Thus, the naphthalene rings of the mono-dehydrogenated DBDMN monomers become well-resolved by nc-AFM imaging, and the line-featured C–Cu–C bonds turn out to be visible, which show a good agreement with the simulated nc-AFM image of mono-dehydrogenated MOCs (Fig. 3b).

After prolonged annealing at room temperature for ~12 hours, the original MOCs undergo a structural rearrangement and transform into a relaxed isomeric form. The same dehydrogenation routine was conducted to unveil the internal structure of relaxed MOCs. In a partially relaxed MOC shown in Fig. 3b, the relaxed part consists of one Cu adatom coordinated to one C(Br) radical site and one C(H) radical site (Fig. 3c). These findings indicate that the relaxed MOC junctions can be derived from strained MOCs by shifting the Cu coordination centre from C(Br) to an adjacent C(H) site, and shifting a H atom from the C(H) to the formerly Cu-bound C(Br) site (Fig. 3a). In addition, the DFT-predicted Cu–Cu distance shows good agreement with the experimental results (7.6 Å and 6.9 Å for strained/relaxed chains). Moreover, the total energy of relaxed MOCs is predicted to be ~0.28 eV lower than that of the strained ones. All these observations indicate that the strain in the original MOCs provides the driving force for the isomeric transformation process.

We also performed a series of calculations including Quantum mechanics/Molecule mechanics and Molecular dynamics simulations to investigate the energy profile of the skeleton rearrangement process in this system. The most energetically favourable rearrangement pathway involves a two-step process with two activation barriers (Fig. 3e–i and k). The first step is a rapid 1,3-H shift proceeding along the $\delta H = h_3 - h_1$ reaction coordinate. Note that the strain stored within the C–Cu bonds increases the transition rate and facilitates the reaction by overcoming an activation barrier of 1.18 eV. The second reaction step involves the dissociation of the C_1–Cu bond and the formation of a new C_3–Cu bond, described by the bond distance as the reaction coordinate, Δ(Cu–C). This step is facilitated by releasing the strain within the chain and a vertical movement (~0.4 Å) of the naphthalene unit to overcome the activation barrier of 0.78 eV (Fig. 3l). Different from conventional approaches, which often require thermal treatment to cleave C–Cu bonds or activate C–H bonds on catalytic substrates, the strain stored within the 1D-MOC system allows for the activation of these chemical transformation processes at room temperature.

Substrate-promoted molecular bonding functionalization

Chi and co-workers reported the site-selective functionalisation of the chemical groups within a single molecule. 4,4″-Diamino-*p*-terphenyl (DATP) molecules with two identical amine groups were studied on the Cu(111) surface. Upon deposition at below 100 K, the nc-AFM images reveal that the DATP molecules adopt two adsorption configurations (Type I and II) on the Cu(111) substrate (Fig. 4b and c). 77.6% of the DATP molecules are found to adopt the Type I adsorption, while the rest of them show the Type II adsorption, which suggests that Type I is the more energetically favourable configuration. Interestingly, the Type II configuration shows a highly symmetric feature in the AFM image, while Type I always appears to have a fuzzy end at one of the amine groups. Additionally, both configurations can be switched back and forth by atomic manipulation. High-resolution nc-AFM images and DFT calcu-

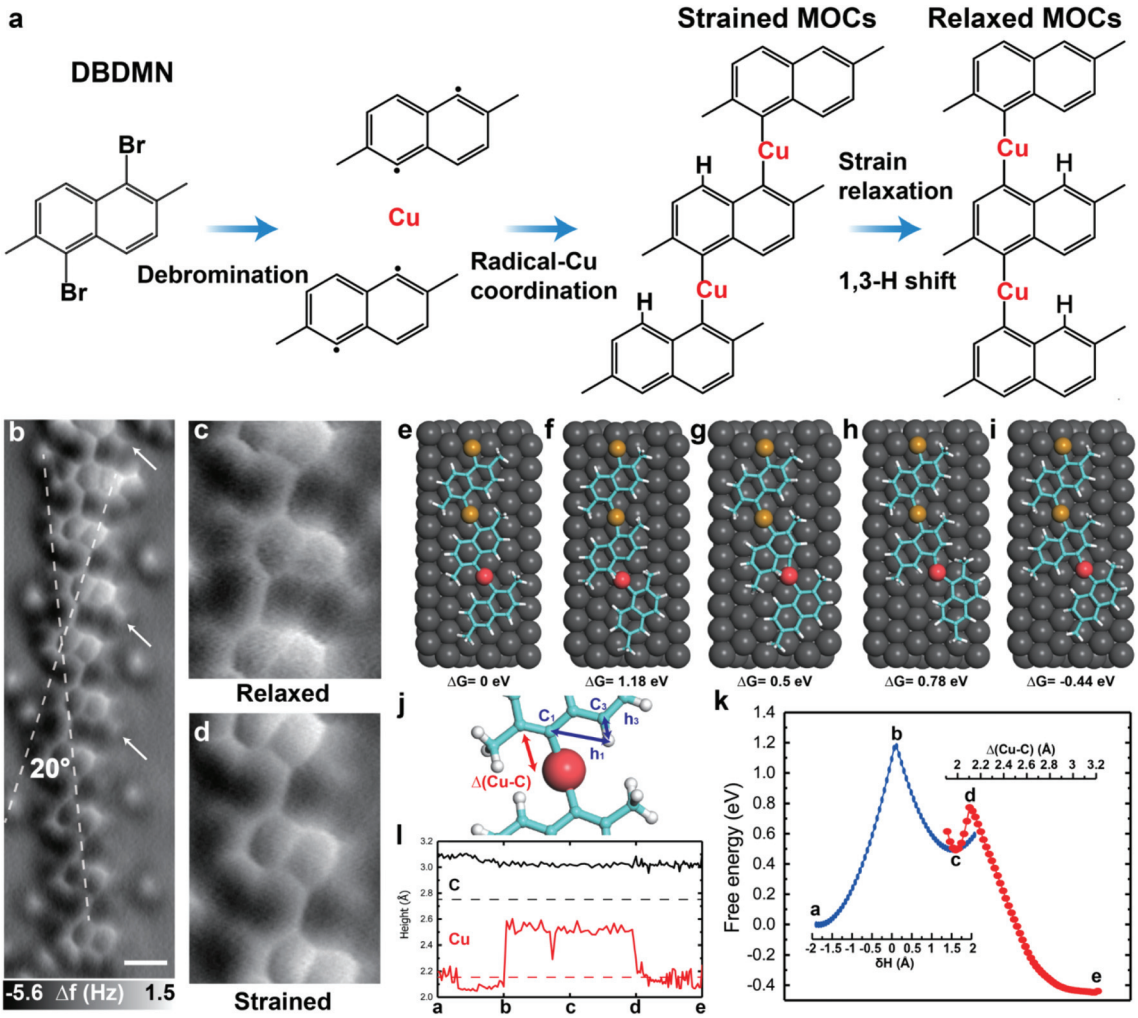

Fig. 3 (a) Schematic illustration of the synthesis and structural relaxation of MOCs on Cu(111). (b) nc-AFM image of the 1D MOC chain with strained and relaxed registry. (c) and (d) nc-AFM image of the same 1D chain in (b) after tip-induced dehydrogenation. (e)–(i) Top view of the structures at different stages of the reaction. (j) Schematic definition of the distances and atoms participating in the reaction. (k) Free energy profile of the two-step reaction. The first part goes through the reaction coordinate $\delta H = h_3 - h_1$ and the second part goes through Δ(Cu–C). (l) Height of the Cu adatom implied in the reaction in red and the average heights of C atoms in black during the reaction at 300 K (relaxed at 0 K in dashed lines). Scale bar: 5 Å. (Reproduced from ref. 48, Copyright 2019, with permission of John Wiley and Sons.)

lations reveal that Type I has two metastable adsorption subtypes (IA and IB), which are separated by ~90 pm from each other on the Cu(111) surface. As illustrated in Fig. 4d and e, the left amino group of Type IA is located close to a top site, while the right amino group lies in close proximity to a fcc hollow site of the Cu(111) surface. As to Type IB, the left amino group is located above an hcp hollow site, while the right amino group is located close to a top site. DFT calculations further reveal that the amino group of the DATP molecule is significantly bent down (~70 pm) towards the surface when it locates above a Cu top site. The downward bending of amino groups indicates the bond formation between the molecule and underlying Cu atoms, which also results in weakened N–H bonds within the amino group. Thus, the fuzzy feature is generated due to additional attraction force at the bent-down amino site which promotes the jumping between Type IA and IB.

A subsequent control experiment was conducted on the Au(111) surface to understand how the substrate interacts with DATP molecules. Interestingly, only one adsorption configuration without any fuzzy feature is observed on the Au(111) surface (Fig. 4h). Both terminal amino groups are located close to the top sites of Au atoms. In addition, the lattice mismatch between DAPH and the Au(111) surface is reduced compared to Cu(111). These observations suggest that the lattice mismatch could be utilized to break the intrinsic symmetry of chemically-equivalent functional groups within a single molecule. In this regard, additional TPCA molecules were deposited onto the DATP/Cu(111) system to investigate the assembling preference of DATP molecules. The nc-AFM images reveal that the TPCA molecules tend to form clusters with Type I at the fuzzy ends, whereas TPCA molecules are always connected with both sides of Type II. This suggests that the bent-down amino groups (fuzzy end of Type I and both ends of Type II)

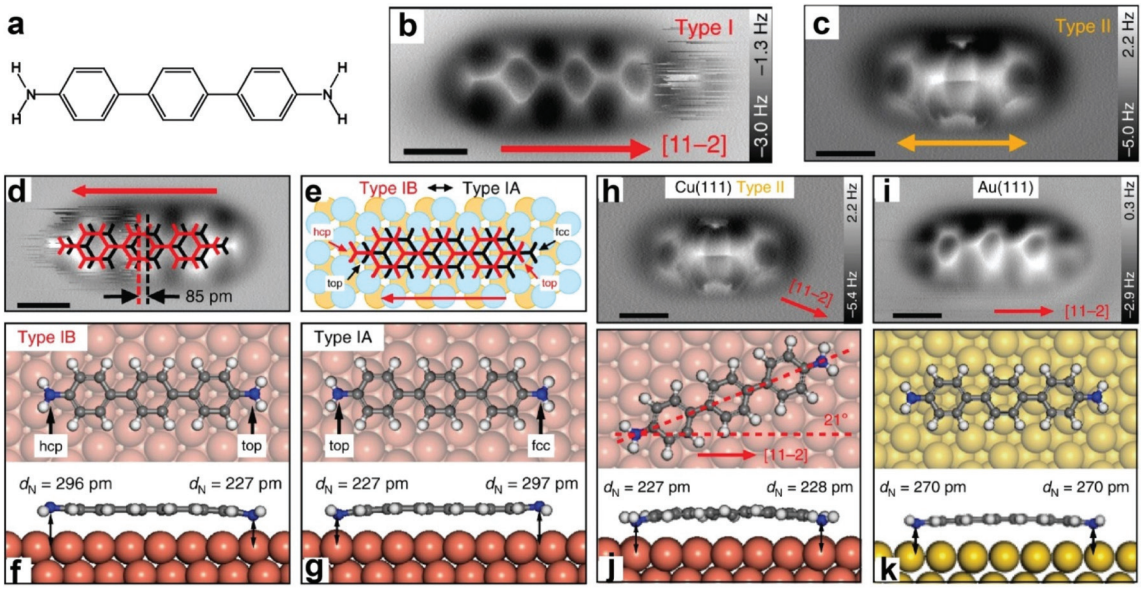

Fig. 4 (a) Chemical structure of DATP. (b and c) Constant height AFM images of molecules with the Type I and Type II adsorption structures. (d) AFM image of DATP type I fitted by two molecular models, namely Type IA (black) and Type IB (red). (e) The sketch of precise adsorption positions as revealed by AFM imaging. The two structures are displaced by 96 pm along the [11−2] direction. (f and g) DFT calculations of the adsorption positions of Type IA and Type IB on Cu(111). (h) AFM image of DATP Type II on Cu(111). (i) AFM image of DATP on Au(111). (j and k) DFT calculations of the corresponding adsorption structures on Cu(111) and Au (111), respectively. (Reproduced from ref. 49, Copyright 2018, with permission of Springer Nature.)

possess a higher binding affinity with TCPA molecules, which could further influence the chemical reactivity of the molecule. The interaction between the nitrogen lone pair and the Cu atoms can weaken the N–H bonds of the amino groups this side. Therefore, the DATP molecule will readily move towards to a nearby TPCA molecule close to the fuzzy site (low energy barrier 5–6 meV).

Perspective

The utilization of strain to promote on-surface chemical reactions emerges as an appealing approach to extend the toolbox of on-surface synthesis for fabricating a wide range of novel molecules and functional nanostructures. The state-of-the-art scanning probe techniques (*e.g.* AFM imaging with a CO-decorated tip or bond-resolved STM) can be used to resolve the chemical backbones of precursors, reaction intermediates and reaction products at an atomic bond level, which provides deep insights into the role of substrate-induced strain in different reaction pathways. In addition, the controllable atomic manipulation assists the removal of out-of-plane atoms without damaging initial backbone conformations for the high-resolution real-space visualization of non-planar chemical structures on the surface. In combination with DFT calculations, it is possible to understand the mechanism of strain-induced on-surface chemical reactions in a comprehensive manner.

Nevertheless, unlike conventional on-surface synthesis, more efforts are needed to exploit the concept of strain-induced reactions for surface chemical transformations. It is highly desirable to apply this approach for the synthesis of more complex functional nanostructures on the surface. Furthermore, it is of great interest to investigate how to control the substrate–adsorbate interactions and the reactivity of a molecular precursor for the fabrication of novel nanostructures. For instance, the DATP molecule exhibits an assembling preference with TPCA on the Cu(111) surface. It is expected that such *in situ* molecular functionalization and assembly strategies could be applied to fabricate different one-dimensional (1D) and two-dimensional (2D) nanostructures in a controllable way.[50] We envision that substrate-induced strain can be harnessed to fabricate a diversity of functional materials and quantum nanostructures for both fundamental research and technology applications.

Conflicts of interest

There are no conflicts to declare.

Acknowledgements

J. Lu acknowledges the support from MOE grants (MOE2017-T2-1-056, R-143-000-A75-114 and R-143-000-B47-114) and the NRF-CRP grant NRF-CRP16-2015-02.

References

1 A. Gourdon, *Angew. Chem., Int. Ed.*, 2008, **47**, 6950–6953.
2 L. Grill, M. Dyer, L. Lafferentz, M. Persson, M. V. Peters and S. Hecht, *Nat. Nanotechnol.*, 2007, **2**, 687–691.
3 J. Cai, P. Ruffieux, R. Jaafar, M. Bieri, T. Braun, S. Blankenburg, M. Muoth, A. P. Seitsonen, M. Saleh, X. Feng, K. Müllen and R. Fasel, *Nature*, 2010, **466**, 470–473.
4 M. Bieri, S. Blankenburg, M. Kivala, C. A. Pignedoli, P. Ruffieux, K. Müllen and R. Fasel, *Chem. Commun.*, 2011, **47**, 10239–10234.
5 C. Janiak and J. K. Vieth, *New J. Chem.*, 2010, **34**, 2366–2324.
6 S. Stepanow, N. Lin and J. V. Barth, *J. Phys.: Condens. Matter*, 2008, **20**, 184002–184016.
7 J. Cai, C. A. Pignedoli, L. Talirz, P. Ruffieux, H. Söde, L. Liang, V. Meunier, R. Berger, R. Li, X. Feng, K. Müllen and R. Fasel, *Nat. Nanotechnol.*, 2014, **9**, 896–900.
8 S. Saito, S. Osumi, S. Yamaguchi, A. S. Foster, P. Spijker, E. Meyer and S. Kawai, *Nat. Commun.*, 2015, **6**, 8098.
9 A. Kimouche, M. M. Ervasti, R. Drost, S. Halonen, A. Harju, P. M. Joensuu, J. Sainio and P. Liljeroth, *Nat. Commun.*, 2015, **6**, 10177.
10 G. D. Nguyen, H.-Z. Tsai, A. A. Omrani, T. Marangoni, M. Wu, D. J. Rizzo, G. F. Rodgers, R. R. Cloke, R. A. Durr, Y. Sakai, F. Liou, A. S. Aikawa, J. R. Chelikowsky, S. G. Louie, F. R. Fischer and M. F. Crommie, *Nat. Nanotechnol.*, 2017, **12**, 1077–1082.
11 D. J. Rizzo, G. Veber, T. Cao, C. Bronner, T. Chen, F. Zhao, H. Rodriguez, S. G. Louie, M. F. Crommie and F. R. Fischer, *Nature*, 2018, **560**, 204–208.
12 S. Kawai, S. Nakatsuka, T. Hatakeyama, R. Pawlak, T. Meier, J. Tracey, E. Meyer and A. S. Foster, *Sci. Adv.*, 2018, **4**, eaar7181.
13 P. Ruffieux, S. Wang, B. Yang, C. Sánchez-Sánchez, J. Liu, T. Dienel, L. Talirz, P. Shinde, C. A. Pignedoli, D. Passerone, T. Dumslaff, X. Feng, K. Müllen and R. Fasel, *Nature*, 2016, **531**, 489–492.
14 L. Talirz, H. Söde, T. Dumslaff, S. Wang, J. R. Sanchez-Valencia, J. Liu, P. Shinde, C. A. Pignedoli, L. Liang, V. Meunier, N. C. Plumb, M. Shi, X. Feng, A. Narita, K. Müllen, R. Fasel and P. Ruffieux, *ACS Nano*, 2017, **11**, 1380–1388.
15 O. Gröning, S. Wang, X. Yao, C. A. Pignedoli, G. Borin Barin, C. Daniels, A. Cupo, V. Meunier, X. Feng, A. Narita, K. Müllen, P. Ruffieux and R. Fasel, *Nature*, 2018, **560**, 209–213.
16 S. Clair and D. G. de Oteyza, *Chem. Rev.*, 2019, **119**, 4717–4776.
17 L. Zhi and K. Müllen, *J. Mater. Chem.*, 2008, **18**, 1472–1413.
18 Y.-Z. Tan, B. Yang, K. Parvez, A. Narita, S. Osella, D. Beljonne, X. Feng and K. M. U. llen, *Nat. Commun.*, 2016, **4**, 1–7.
19 Y.-C. Chen, T. Cao, C. Chen, Z. Pedramrazi, D. Haberer, D. G. de Oteyza, F. R. Fischer, S. G. Louie and M. F. Crommie, *Nat. Nanotechnol.*, 2015, **10**, 156–160.
20 M. Treier, C. A. Pignedoli, T. Laino, R. Rieger, K. Müllen, D. Passerone and R. Fasel, *Nat. Chem.*, 2011, **3**, 61–67.
21 L. Talirz, P. Ruffieux and R. Fasel, *Adv. Mater.*, 2016, **28**, 6222–6231.
22 N. Pavliček, A. Mistry, Z. Majzik, N. Moll, G. Meyer, D. J. Fox and L. Gross, *Nat. Nanotechnol.*, 2017, **12**, 308–311.
23 J. Su, M. Telychko, P. Hu, G. Macam, P. Mutombo, H. Zhang, Y. Bao, F. Cheng, Z.-Q. Huang, Z. Qiu, S. J. R. Tan, H. Lin, P. Jelínek, F.-C. Chuang, J. Wu and J. Lu, *Sci. Adv.*, 2019, **5**, eaav7717–eaav7777.
24 L. Lafferentz, V. Eberhardt, C. Dri, C. Africh, G. Comelli, F. Esch, S. Hecht and L. Grill, *Nat. Chem.*, 2012, **4**, 215–220.
25 Y. Cao, J. Qi, Y.-F. Zhang, L. Huang, Q. Zheng, X. Lin, Z. Cheng, Y.-Y. Zhang, X. Feng, S. Du, S. T. Pantelides and H.-J. Gao, *Nano Res.*, 2018, **11**, 6190–6196.
26 J. I. Urgel, S. Mishra, H. Hayashi, J. Wilhelm, C. A. Pignedoli, M. Di Giovannantonio, R. Widmer, M. Yamashita, N. Hieda, P. Ruffieux, H. Yamada and R. Fasel, *Nat. Commun.*, 2019, **10**, 861.
27 K. A. Simonov, N. A. Vinogradov, A. S. Vinogradov, A. V. Generalov, E. M. Zagrebina, G. I. Svirskiy, A. A. Cafolla, T. Carpy, J. P. Cunniffe, T. Taketsugu, A. Lyalin, N. Mårtensson and A. B. Preobrajenski, *ACS Nano*, 2015, **9**, 8997–9011.
28 M. Bieri, M.-T. Nguyen, O. Gröning, J. Cai, M. Treier, K. Aït-Mansour, P. Ruffieux, C. A. Pignedoli, D. Passerone, M. Kastler, K. Müllen and R. Fasel, *J. Am. Chem. Soc.*, 2010, **132**, 16669–16676.
29 M. Treier, C. A. Pignedoli, T. Laino, R. Rieger, K. Müllen, D. Passerone and R. Fasel, *Nat. Chem.*, 2011, **3**, 61–67.
30 O. Stetsovych, M. Švec, J. Vacek, J. V. Chocholoušová, A. Jančařík, J. Rybáček, K. Kosmider, I. G. Stará, P. Jelínek and I. Starý, *Nat. Chem.*, 2016, **9**, 213–218.
31 J. R. Sanchez-Valencia, T. Dienel, O. Gröning, I. Shorubalko, A. Mueller, M. Jansen, K. Amsharov, P. Ruffieux and R. Fasel, *Nature*, 2014, **512**, 61–64.
32 G. Vasseur, Y. Fagot Revurat, M. Sicot, B. Kierren, L. Moreau, D. Malterre, L. Cardenas, G. Galeotti, J. Lipton-Duffin, F. Rosei, M. Di Giovannantonio, G. Contini, P. Le Fèvre, F. Bertran, L. Liang, V. Meunier and D. F. Perepichka, *Nat. Commun.*, 2016, **7**, 10235.
33 J. Björk, S. Stafström and F. Hanke, *J. Am. Chem. Soc.*, 2011, **133**, 14884–14887.
34 A. Shiotari, T. Nakae, K. Iwata, S. Mori, T. Okujima, H. Uno, H. Sakaguchi and Y. Sugimoto, *Nat. Commun.*, 2017, **8**, 16089.
35 F. J. Giessibl, *Rev. Mod. Phys.*, 2003, **75**, 949–983.
36 L. Gross, *Nat. Chem.*, 2011, **3**, 273–278.
37 A. Riss, A. P. Paz, S. Wickenburg, H.-Z. Tsai, D. G. de Oteyza, A. J. Bradley, M. M. Ugeda, P. Gorman, H. S. Jung, M. F. Crommie, A. Rubio and F. R. Fischer, *Nat. Chem.*, 2016, **8**, 678–683.
38 N. Pavliček and L. Gross, *Nat. Rev. Chem.*, 2017, **1**, 0005–0011.

39 N. Pavliček, P. Gawel, D. R. Kohn, Z. Majzik, Y. Xiong, G. Meyer, H. L. Anderson and L. Gross, *Nat. Chem.*, 2018, **10**, 853–858.
40 F. J. Giessibl, *Rev. Sci. Instrum.*, 2019, **90**, 011101.
41 L. Gross, F. Mohn, N. Moll, P. Liljeroth and G. Meyer, *Science*, 2009, **325**, 1110–1114.
42 F. Mohn, B. Schuler, L. Gross and G. Meyer, *Appl. Phys. Lett.*, 2013, **102**, 073109–073105.
43 N. Moll, L. Gross, F. Mohn, A. Curioni and G. Meyer, *New J. Phys.*, 2010, **12**, 125020–125016.
44 P. Hapala, G. Kichin, C. Wagner, F. S. Tautz, R. Temirov and P. Jelínek, *Phys. Rev. B*, 2014, **90**, 1989–1989.
45 D. G. de Oteyza, P. Gorman, Y.-C. Chen, S. Wickenburg, A. Riss, D. J. Mowbray, G. Etkin, Z. Pedramrazi, H.-Z. Tsai, A. Rubio, M. F. Crommie and F. R. Fischer, *Science*, 2013, **340**, 1434–1437.
46 N. Pavliček, B. Schuler, S. Collazos, N. Moll, D. Pérez, E. Guitián, G. Meyer, D. Peña and L. Gross, *Nat. Chem.*, 2015, **7**, 623–628.
47 N. Pavliček, Z. Majzik, S. Collazos, G. Meyer, D. Pérez, E. Guitián, D. Peña and L. Gross, *ACS Nano*, 2017, **11**, 10768–10773.
48 M. Telychko, J. Su, A. Gallardo, Y. Gu, J. I. Mendieta-Moreno, D. Qi, A. Tadich, S. Song, P. Lyu, Z. Qiu, H. Fang, M. J. Koh, J. Wu, P. Jelínek and J. Lu, *Angew. Chem., Int. Ed. Engl.*, 2019, **58**, 18591–18597.
49 Q. Zhong, D. Ebeling, J. Tschakert, Y. Gao, D. Bao, S. Du, C. Li, L. Chi and A. Schirmeisen, *Nat. Commun.*, 2018, **9**, 3277.
50 J. Liu, Q. Chen, K. Cai, J. Li, Y. Li, X. Yang, Y. Zhang, Y. Wang, H. Tang, D. Zhao and K. Wu, *Nat. Commun.*, 2019, **10**, 2545.